

Joint ADS-B in B5G for Hierarchical UAV Networks: Performance Analysis and MEC Based Optimization

Chao Dong, *Senior Member, IEEE*, Yiyang Liao, Ziyue Jia, *Member, IEEE*,
Qihui Wu, *Fellow, IEEE*, and Lei Zhang

Abstract—Unmanned aerial vehicles (UAVs) play significant roles in multiple fields, which brings great challenges for the airspace safety. In order to achieve efficient surveillance and break the limitation of application scenarios caused by single communication, we propose the collaborative surveillance model for hierarchical UAVs based on the cooperation of automatic dependent surveillance-broadcast (ADS-B) and 5G. Specifically, UAVs are hierarchical deployed, with the low-altitude central UAV equipped with the 5G module, and the high-altitude central UAV with ADS-B, which helps automatically broadcast the flight information to surrounding aircraft and ground stations. Firstly, we build the framework, derive the analytic expression, and analyze the channel performance of both air-to-ground (A2G) and air-to-air (A2A). Then, since the redundancy or information loss during transmission aggravates the monitoring performance, the mobile edge computing (MEC) based on-board processing algorithm is proposed. Finally, the performances of the proposed model and algorithm are verified through both simulations and experiments. In detail, the redundant data filtered out by the proposed algorithm accounts for 53.48%, and the supplementary data accounts for 16.42% of the optimized data. This work designs a UAV monitoring framework and proposes an algorithm to enhance the observability of trajectory surveillance, which helps improve the airspace safety and enhance the air traffic flow management.

Index Terms—UAV, ADS-B, beyond 5G, mobile edge computing, stochastic geometry.

I. INTRODUCTION

WITH the rapid development of aviation technologies, unmanned aerial vehicles (UAVs) are widely popularized. Due to the reliability, flexibility, adaptability, and high efficiency, UAVs are extensively applied in many fields, including the aerial photography, urban logistics, environmental monitoring, and UAV-assisted vehicular networks [1]. However, as the number of UAVs increases, the flight safety becomes a non-negligible problem. Hence, it is necessary to strengthen the flight control and safety supervision to guarantee that the flight operation of UAVs does not affect the public safety and personal privacy [2]. To deal with such problems, we consider joint the automatic dependent

surveillance-broadcast (ADS-B) technique [3] in 5G, to realize the collaborative surveillance in the beyond 5G (B5G) networks.

The ADS-B system is composed of multiple ground stations (GSs) and airborne stations, which works at a specific frequency band, i.e., 1090MHz. Furthermore, the main service information of ADS-B includes the aircraft position, aircraft identification, aircraft velocity, and flight direction. In detail, an aircraft equipped with ADS-B can automatically broadcast its flight information to the nearby aircraft and GSs, which is conducive to the flight safety and air traffic management [4]. However, due to the limited frequency band, excessive UAVs equipped with ADS-B interfere in the surveillance of GS towards civil planes. The typical impact is intensifying the collision of ADS-B packets, which leads to packets loss, and impairs the monitoring performance of GS towards civil planes [5]. In order to weaken the hindrance on monitoring performance, ensure timely acquisition of the flight information of UAVs, and expand the monitoring capacity of GS, we consider the cooperation of ADS-B with 5G.

Leveraging 5G to establish the network connection has the characteristics of ultra-high speed, ultra-low delay and ultra-large bandwidth [6], which meets the requirements for the wireless communication performance for UAV control and flight missions [7]. UAVs equipped with 5G modules achieve real-time interactions between UAVs and GSs [8]. However, single utilization of 5G brings the difficulties in the long distance transmission, and the integration of the network and air traffic management system of civil aviation. Therefore, we propose to deploy 5G modules on UAVs, by cooperating with ADS-B, to help GS acquire timely flight information. Besides, the central UAVs are equipped with computing resources, to handle the problem of trajectory optimization.

The deployment of UAVs adopts a hierarchical management structure [9]. Besides, the mobile edge computing (MEC) modules are equipped on the central UAVs. In particular, the flight information of sub-UAVs is initially relayed to the central UAVs, and then transmitted to GS after MEC based processing. Due to the hierarchical structure, there exist two communication channels, i.e., the air-to-air (A2A) channel and air-to-ground (A2G) channel. To be specific, the A2A channel is established between the central UAV and sub-UAVs, while the A2G channel provides connections between the central UAV and GS.

The challenges lie in how to construct the hierarchical

Chao Dong, Yiyang Liao, Qihui Wu and Lei Zhang are with the College of Electronic and Information Engineering, Nanjing University of Aeronautics and Astronautics, Nanjing 211106, China (e-mail: dch@nuaa.edu.cn; liaoyiyang@nuaa.edu.cn; wuqihui@nuaa.edu.cn; Zhang_lei@nuaa.edu.cn).

Ziyue Jia is with the College of Electronic and Information Engineering, Nanjing University of Aeronautics and Astronautics, Nanjing 211106, China, and also with the National Mobile Communications Research Laboratory, Southeast University, Nanjing, Jiangsu, 211111, China (e-mail: jiaziyue@nuaa.edu.cn).

monitoring surveillance for UAVs, carry out the channel performance analyze, and handle the problem of trajectory optimization. Hence, the contributions of this paper are summarized as follows:

- A cooperation framework of ADS-B and 5G for hierarchical UAV networks is designed to achieve the UAV flight information, aiming to improve the airspace safety and enhance the air traffic flow management.
- We establish the A2A channel and A2G channel by stochastic modeling and deterministic modeling, respectively. Besides, we carry out the relevant analysis.
- We propose the algorithm of on-board processing based on MEC, which can abandon redundant packets and supply missed packets, to increase the observability.
- Extensive simulations are conducted to verify the influence of the height, density, path loss and transmitting power on the performance of the proposed network. Besides, we conduct real experiments to collect position packets for algorithm verification.

The rest of this paper is organized as follows. Section II elaborates the related works. Besides, the network system model is introduced in Section III. Moreover, the stochastic performance analysis is presented in Section IV. Additionally, Section V describes the mechanisms of on-board processing based on MEC. Section VI provides the simulation results and corresponding analyses. Finally, Section VII draws the conclusions.

II. RELATED WORKS

A. ADS-B, 5G, and MEC

There exist some works about UAV equipped with ADS-B or 5G. For example, Ref. [4] designs a system for UAV surveillance based on ADS-B and proposes related algorithms to handle trajectory planning. Ref. [6] analyzes the impact of UAVs equipped with ADS-B on the civil planes at the frequency of 1090MHz, verifying the access capacity of the network layer. Ref. [8] points out that 5G fully meets the requirements for the wireless communication performance of UAVs flight control and missions, achieving real-time interaction between UAVs and GS. Ref. [10] develops a novel trust-based security scheme for 5G UAV communication systems, improving the communication performance and evaluating the reliability. Besides, there exist some related works about the deployment of the MEC on UAVs, aiming to improve the performance of UAV communications by appropriately utilizing computing resources at the edge of networks [11]. For example, Ref. [12] considers a task offloading problem for a UAV-assisted MEC system, and designs an integrated cloud-edge network, thus minimizing the weighted cost of latency and energy consumption. Ref. [13] proposes a joint communication and computation optimization network model of UAV swarms, which leverages MEC to decrease the response delay and increase the efficiency of network resources utilization. Ref. [14] designs a UAV-assisted MEC system to verify the UAV trajectory optimization, resource allocation, and tasks offloading. The work handles the problem of minimizing the energy consumption of mobile devices and computing power

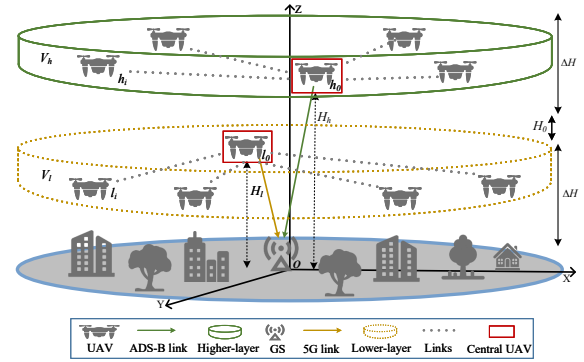


Fig. 1. Hierarchical UAV network model.

of UAVs. Ref. [15] utilizes the resources of computation and storage on UAVs to propose an elastic collaborative MEC intelligence, enhancing the network instability.

B. Channel Modeling

Additionally, there exist some works involving the establishment of channel models related with UAVs. For example, Ref. [16] points out that channel modeling has two methods, including deterministic modeling and stochastic modeling. The deterministic modeling has significant precision but lacks universality. On the contrary, the stochastic modeling is flexible but lacks pertinence. Ref. [17] employs a deterministic channel model that simply abstracts the physical layer, and effectively captures the effects of channel strength, broadcast and superposition in wireless channels. Ref. [18] leverages deterministic model to investigate the optimization for massive multi-input multi-output near-field wireless communications in respect to line-of-sight (LOS) channel. Ref. [19] states that UAV wireless networks have natural spatial random characteristics and the channel has fading and shadowing characteristics. Hence, the stochastic modeling is based on the theory of the stochastic geometry (SG). Ref. [20] leverages the Poisson point process (PPP) in SG to simulate the distribution of the coexistence of UAVs and planes, aiming to analyze the signal interference. The authors in Ref. [13] utilize SG to analyze the response delay and the successful transmission probability of the UAV network, and deduce the analytical form of signal-to-interference-plus-noise ratio (SINR).

C. State of the Art

As far as the authors know, apart from ADS-B and 5G, there are other ways to establish the communication, so as to achieve timely surveillance. Ref. [21] points out that, based on Bluetooth or WiFi, Remote ID is a broadcast technology that offers the identification and position information of UAVs [22]. Besides, Ad-hoc is a kind of temporary network that does not rely on traditional infrastructure [23]. It directly establishes communication with peers [24]. Moreover, incorporating UAVs with satellite communication systems overcomes the geographical limitations [25]. However, all the demands faced by the aforementioned technologies can be met by ADS-B and 5G, which cover the long-distance, short-distance,

TABLE I
KEY PARAMETERS

Notation	Definition
λ_l/λ_h	The density of low/high-altitude UAVs
V_l/V_h	The low/high-altitude airspace
l_0/h_0	The central UAV of low/high-altitude airspace
l_j/h_i	The sub-UAVs of low/high-altitude airspace
H_l/H_h	The height of l_0/h_0
d_{l_j}/d_{h_i}	The distance between l_j/h_i and l_0/h_0
ΔH	The thickness of the airspace
P_{cl}/P_{ch}	The transmitting power of l_0/h_0
P_s	The transmitting power of all sub-UAVs
G_a/G_g	The total gain of A2A/A2G channel
$\Delta\varphi$	The difference of phase between paths
ψ	The grazing angle of signal
\mathcal{D}	The divergence factor
Γ_{\perp}/Γ_t	The reflection coefficient without/with the influence of \mathcal{D}
$ \Gamma_t /\phi_t$	The length/phase of Γ_t
$\lambda_{5G}/\lambda_{ADS-B}$	The wavelength of 5G/ADS-B signal
f_{5G}/f_{ADS-B}	The frequency of 5G/ADS-B signal
B_{5G}/B_{ADS-B}	The bandwidth of 5G/ADS-B signal
$\varepsilon_0/\varepsilon_r$	The dielectric constant/The relative dielectric constant
σ	The electric conductivity
PL	The path loss of A2G channel (dB)
ϖ	SNR between the central UAV and GS
N_0/n_0	Gaussian noise/The power density of noise
δ	The index of path loss in A2A
ρ	The index of small scale fading in A2A
γ	SINR between the central UAV and sub-UAV
θ_l/θ_h	The received threshold of l_0/h_0
P_{cov}	The coverage probability
$I_{l_j}^g/I_{h_i}^k$	The g -th/ k -th 5G/ADS-B packet from the j -th/ i -th sub-UAV
$Lon_{h_i}^k/Lat_{h_i}^k/Alt_{h_i}^k$	The longitude/latitude/altitude information of $I_{h_i}^k$
\mathcal{M}_{h_i}	The vector of Minkowski for h_i
$m_{h_i}^n$	The n -th Minkowski distance in \mathcal{M}_{h_i}
X/\hat{B}	The coefficient/constant determinant

high-speed and low-latency communications. Therefore, we innovatively utilize ADS-B in 5G to build the hierarchical UAV networks, which guarantees the integrated management by civil aviation authorities, and achieves various applications in different scenarios, aiming to propose a safe collaborative surveillance with respect to hierarchical UAV networks.

Traditional trajectory optimization involves two major problems, i.e., trajectory planning and trajectory prediction, and mainly adopts methods such as particle filtering [26], Kalman filtering [27], and neural networks [28]. However, in this paper, the trajectory optimization focuses on the problem of monitoring observability, which values timeliness over accuracy. Therefore, we designed the on-board processing algorithm, inspired by the sliding window filtering, to improve the observability and solve a practical engineering problem.

III. SYSTEM MODEL

Fig. 1 depicts the hierarchical UAV network model. In detail, a group of UAVs with density λ_l are randomly distributed in the low-altitude airspace V_l , corresponding to the orange dotted line area. Another group of UAVs with density λ_h scatter in the high-altitude airspace V_h , as the green solid line area shows. Besides, a central UAV exists in each layer. The low-altitude central UAV is equipped with 5G module, while the high-altitude central UAV transmits the flight information through the ADS-B system. H_h and H_l are regarded as the altitude of the central UAV h_0 and central UAV l_0 , respectively. ΔH is the height of both airspaces. Furthermore,

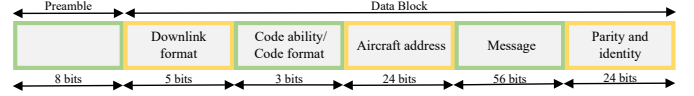


Fig. 2. Structure of ADS-B.

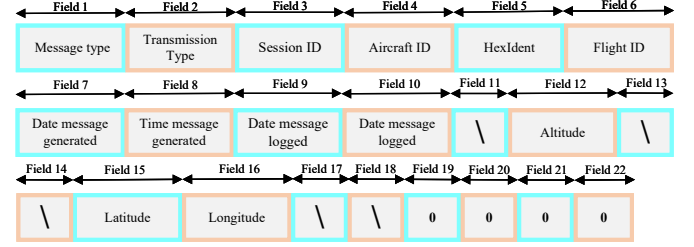


Fig. 3. Structure of airborne position TM.

there is an isolation layer with height H_0 between the two airspaces, aiming to reduce the interference among the UAVs from different airspaces. It is assumed that there is a GS located at $\mathbf{O}(0, 0, 0)$ in the space. GS can receive the 5G flight information from l_0 and the ADS-B flight information from h_0 . Additionally, since the central UAVs serve as aerial stations, which are quasi-static, we establish the A2G channels by utilizing deterministic models, which have the merits of strong pertinence, precise fit and high accuracy. Besides, considering the mobility and maneuverability of sub-UAVs, we establish the A2A channels by leveraging stochastic models, which have the advantages of universality and flexibility. Key parameters and corresponding definitions are summarized in TABLE I.

A. Data Format

1) *Data Format of ADS-B*: As shown in Fig. 2, a single ADS-B data consists of an 8-bit preamble and a 112-bit data block [29]. The down link format (DF) is 5 bits long, which is used to distinguish the type of transponder. If DF=17, the third field is the code ability. If DF=18, the third field is the code format. Besides, the aircraft address field is 24 bits long. The message field contains the service information. Finally, the length of parity and identity field is 24 bits [30].

2) *Data Format of 5G*: To facilitate the information processing of GS, we transmit the Kinetic Avionics data via the 5G network, and the specific data format is compatible with ADS-B. In this work, we primarily focus on the longitude, latitude and altitude information. Therefore, we utilize the airborne position message, illustrated in Fig. 3. Specifically, field 1 is the fixed character, i.e., "MSG". The transmission type is set as "3", corresponding to the airborne position message. Fields 3 and 4 indicate the database session record number and database aircraft record number, respectively. Besides, field 5 represents the aircraft mode S hexadecimal code and field 6 symbolizes the database flight record number. The meanings of other fields are shown in the Fig. 3. Moreover, a slash denotes that the field is empty, and the last four fields are fixed as "0" in respect to the airborne position message [31].

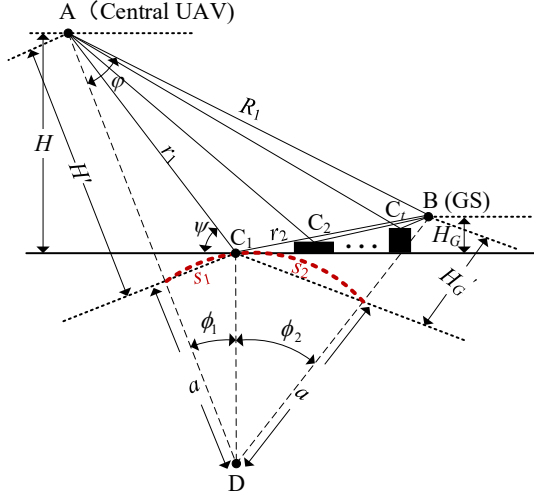


Fig. 4. A2G channel.

B. Parameters of UAV Model

Denote the set of high-altitude UAVs as $\mathcal{H} = \{h_0, h_1, \dots, h_i, \dots, h_u\}$ and $i \in (1, u)$. Indicate the set of low-altitude UAVs as $\mathcal{L} = \{l_0, l_1, \dots, l_j, \dots, l_v\}$ and $j \in (1, v)$. u and v represent the number of the corresponding sub-UAVs. In detail, h_0 in \mathcal{H} symbolizes the central UAV in the high-altitude airspace while l_0 in \mathcal{L} indicates the central UAV in the low-altitude airspace. Additionally, the coordinate of the i -th UAV in set \mathcal{H} is $(x_{h_i}, y_{h_i}, z_{h_i})$ and the coordinate of the j -th UAV in set \mathcal{L} is $(x_{l_j}, y_{l_j}, z_{l_j})$. The X-axis coordinates for all UAVs range within $[-L_x, L_x]$, the Y-axis coordinates range within $[-L_y, L_y]$, and the Z-axis coordinates are from $[0, L_z]$. In specific, $L_z = 2\Delta H + H_0$. The euclidean distance between UAV h_i and h_0 is $d_{h_i} = \sqrt{(x_{h_i} - x_{h_0})^2 + (y_{h_i} - y_{h_0})^2 + (z_{h_i} - z_{h_0})^2}$, and the euclidean distance between UAV l_j and l_0 is $d_{l_j} = \sqrt{(x_{l_j} - x_{l_0})^2 + (y_{l_j} - y_{l_0})^2 + (z_{l_j} - z_{l_0})^2}$. P_s represents the transmitting power of the sub-UAV. In addition, P_c declares the transmitting power of the central UAV, which is further divided into P_{ch} of h_0 and P_{cl} of l_0 , respectively. G_g represents the total gain of the A2G channel, including the transmitter gain in the central UAV and receiver gain at GS. Besides, G_a represents the total gain of the A2A channel, including the transmitter gain in sub-UAV and the receiver gain in the central UAV. Besides, P_s , G_g and G_a are same for all links in the model.

C. A2G Channel Model

In the case of long link distances, the shape of earth is approximately equivalent to a sphere of radius a [32]. Therefore, we model the A2G into a curved-earth multi-rays (CEMR) model, as shown in Fig. 4. Moreover, the black rectangles represent the reflectors. The distance of LoS component between A and B is R_1 . Additionally, we take the non-line-of-sight (NLoS) component passing C_1 for example, whose distance is R_2 , and $R_2 = r_1 + r_2$. Furthermore, D is regarded as the center of earth and C_t is supposed to be the t -th reflection point. Initially, we denote the distance between the

central UAV and the surface as H , and assume the distance between the central UAV and the tangential plane at C_1 as H' . Specifically, when concerning the high-altitude airspace, H refers to H_h . Besides, H conducts as H_l when involving the low-altitude airspace. Subsequently, H_G expresses the distance between GS and the surface. H'_G declares the distance between GS and the tangential plane at C_1 . Since we arrange the central UAVs to hover in a small area above the GS, the horizontal distance is ignored in comparison with the vertical distance, i.e., $H \approx H'$ and $H_G \approx H'_G$. In triangle ABD, according to the law of cosine [33], we have

$$R_1^2 = (a + H')^2 + (a + H'_G)^2 - 2(a + H')(a + H'_G) \cos(\phi), \quad (1)$$

where $\phi = \phi_1 + \phi_2$, $s = s_1 + s_2 = a\phi$, $AB = R_1$, $AD = H' + a$, and $BD = H'_G + a$. By substituting the above formulas, three intermediate variables are defined, which are conducive to the simplified exhibition of equations [34]. In detail, three intermediate variables ω_1 , ω_2 , and ω_3 are introduced as

$$\begin{cases} \omega_1 = \frac{s^2}{4a(H' + H'_G)}, \\ \omega_2 = \frac{H' - H'_G}{H' + H'_G}, \\ \omega_3 = 2\sqrt{\frac{\omega_1 + 1}{3\omega_1}} \cos \left\{ \frac{\pi}{3} + \frac{1}{3} \arccos \left[\frac{3\omega_2}{2} \sqrt{\frac{3\omega_1}{(\omega_1 + 1)^3}} \right] \right\}. \end{cases} \quad (2)$$

By combining Eq. (1), (2) and $s = a\phi$, we obtain

$$\begin{cases} s_1 = \frac{s(1 + \omega_3)}{2}, \\ s_2 = s - s_1, \\ \phi_1 = \frac{s_1}{a}. \end{cases} \quad (3)$$

The phase difference of the signal between path AB and path AC_1B is $\Delta\varphi_1$, calculated as

$$\Delta\varphi_1 = \frac{2\pi\Delta s}{\lambda}, \quad (4)$$

where $\Delta s = 2s_1s_2\psi^2/s$, $\psi = (H' + H'_G)[1 - \omega_1(1 + \omega_2^2)]/s$ and λ is the wavelength. In detail, $\lambda = c/f$, in which c is the velocity of light and f is the frequency. Additionally, we assume that the reflection coefficient of earth is Γ_{\perp} . Since we consider all UAVs are equipped with vertically polarized antennas, Γ_{\perp} is simplified as

$$\Gamma_{\perp} = \frac{(\varepsilon_r - jb) \sin \psi - \sqrt{(\varepsilon_r - jb)^2 - \cos^2 \psi}}{(\varepsilon_r - jb) \sin \psi + \sqrt{(\varepsilon_r - jb)^2 - \cos^2 \psi}}, \quad (5)$$

where ε_r is the relative dielectric constant and $j^2 = -1$. Besides, $b = \sigma / (2\pi f \varepsilon_0)$, where σ is the electric conductivity, and ε_0 is the dielectric constant. Nevertheless, the reflection coefficient of point C_1 is $\Gamma_1 = |\Gamma_{\perp}| e^{j\phi_1} = \mathcal{D}\Gamma_{\perp}$, where \mathcal{D} is the divergence factor. Further, \mathcal{D} is defined as

$$\mathcal{D} = \left[1 + \frac{2r_1r_2}{a(r_1 + r_2) \sin \psi} \right]^{-\frac{1}{2}}, \quad (6)$$

where r_1 is obtained from the law of cosine in triangle AC_1D , i.e., $r_1^2 = (a + H')^2 + a^2 - 2a(a + H') \cos \phi_1$ and r_2 is obtained from the law of cosine in triangle C_1BD , i.e., $r_2^2 = (a + H'_G)^2 + a^2 - 2a(a + H'_G) \cos \phi_2$. E_{LoS} and E_{NLoS} respectively symbolize the signal strength of the LoS path and the t -th NLoS path, and $|E_{LoS}|^2 = P_c G_t$, where G_t denotes the

transmitter gain of the central UAV. Hence, the signal strength E_G received by GS is the vector sum of the signals at point B, whose analytic form is

$$\begin{aligned} E_G &= E_{LoS} + \sum_{t=1}^{\lfloor \frac{\pi}{2\varrho} \rfloor} E_{NLoS}t \\ &= E_{LoS} \left[1 + \sum_{t=1}^{\lfloor \frac{\pi}{2\varrho} \rfloor} |\Gamma_t| e^{-j(\Delta\varphi_t - \phi_t)} \right] \\ &= E_{LoS} \left\{ \left[1 + \sum_{t=1}^{\lfloor \frac{\pi}{2\varrho} \rfloor} |\Gamma_t| \cos(\Delta\varphi_t - \phi_t) \right] \right. \\ &\quad \left. - j \sum_{t=1}^{\lfloor \frac{\pi}{2\varrho} \rfloor} |\Gamma_t| \sin(\Delta\varphi_t - \phi_t) \right\}, \end{aligned} \quad (7)$$

where ϱ denotes the beamwidth. Moreover, the power P_G of the signal received by GS is formulated as

$$P_G = \frac{\|E_G\|^2 G_r \lambda^2}{(4\pi R_1)^2}, \quad (8)$$

where G_r is the receiver gain at GS and $G_t G_r = G_g$. Hence, the path loss of the A2G communication system is defined as

$$PL = -10 \log_{10} \left(\frac{P_G}{P_c} \right). \quad (9)$$

Additionally, ϖ denotes the signal-to-noise ratio (SNR), i.e.,

$$\varpi = 10 \log_{10}(P_G) - 10 \log_{10}(n_0 B), \quad (10)$$

where n_0 is the noise power density and B is the bandwidth.

D. A2A Channel Model

Considering the hierarchical airspace, we set up an isolation layer between the airspaces, and only the interference in the same airspace is considered in the model. The sub-UAVs in the same airspace communicate with the central UAV. Considering the high-altitude airspace, the path loss from the i -th sub-UAV to the central UAV is proportional to $d_{h_i}^{-\delta}$, where d_{h_i} denotes the distance between the sub-UAV and central UAV. δ indicates the path loss index. Besides, ρ_{h_i} follows an exponential distribution with mean value of 1, indicating the gain of small scale fading channel. Similarly, Gaussian noise N_0 is added to the model, i.e., $N_0 = n_0 B$. We leverage γ to represent SINR. γ_{h_i} , the desired signal sent by the i -th sub-UAV h_i in set \mathcal{H} to the central UAV h_0 , is calculated as

$$\gamma_{h_i} = \frac{P_s G_a \rho_{h_i} d_{h_i}^{-\delta}}{N_0 + P_s S_{\mathcal{H} \setminus \{h_i\}}}, \quad (11)$$

where

$$S_{\mathcal{H} \setminus \{h_i\}} = \sum_{h \in \mathcal{H} \setminus \{h_i\}} G_a \rho_{h_i} d_{h_i}^{-\delta}. \quad (12)$$

Similarly, as for the low-altitude airspace, SINR γ_{l_j} of the desired signal sent by the j -th sub-UAV l_j in set \mathcal{L} to the central UAV l_0 is

$$\gamma_{l_j} = \frac{P_s G_a \rho_{l_j} d_{l_j}^{-\delta}}{N_0 + P_s S_{\mathcal{L} \setminus \{l_j\}}}, \quad (13)$$

in which

$$S_{\mathcal{L} \setminus \{l_j\}} = \sum_{l \in \mathcal{L} \setminus \{l_j\}} G_a \rho_{l_j} d_{l_j}^{-\delta}. \quad (14)$$

IV. ANALYSIS OF STOCHASTIC GEOMETRY

In this section, we use the PPP in SG theory to fit the distributions of sub-UAVs in the A2A. Besides, the analytic function is derived for the performance analysis. Taking the high-altitude airspace V_h for example, all sub-UAVs follow the nearest neighbor association strategy [35], i.e.,

$$P\{d_h > R^*\} = \exp(-\lambda_h V_h) = \exp\left(-\frac{4}{3}\pi\lambda_h d_h^3\right), \quad (15)$$

where $d_h \geq 0$, and R^* is the longest distance that the central UAV can serve. Therefore, the cumulative distribution function (CDF) of the distance d_h is

$$F(d_h) = P\{d_h \leq R^*\} = 1 - \exp\left(-\frac{4}{3}\pi\lambda_h d_h^3\right), \quad (16)$$

and the probability density function (PDF) of d_h is a derivative of CDF, demonstrated as

$$f(d_h) = 4\pi\lambda_h d_h^2 \exp\left(-\frac{4}{3}\pi\lambda_h d_h^3\right). \quad (17)$$

Supposing the transmission will be successful if the γ_{h_i} is greater than the received threshold θ_h of the central UAV h_0 , so the coverage probability of the i -th sub-UAV in \mathcal{H} is

$$P_{cov}^i = \mathbb{E}[P(\gamma_{h_i} \geq \theta_h | d_{h_i})]. \quad (18)$$

Since γ_{h_i} is a function of d_{h_i} , P_{cov}^i is further expressed as

$$P_{cov}^i = \int_0^\infty P(\gamma_{h_i} \geq \theta_h | d_{h_i}) f(d_h) d(d_h). \quad (19)$$

It is assumed that the average gain of small scale fading channel in the A2A is a random variable following the Gamma distribution with mean value of 1 [36], which is depicted as

$$f(\rho) = \frac{\iota^\iota}{\Gamma(\iota)} \rho^{\iota-1} e^{-\rho}. \quad (20)$$

When ι is 1, the channel is considered as Rayleigh fading. ρ follows an exponential distribution with mean value of 1. The PDF of ρ is $f(x) = e^{-x}$, i.e., $\rho_{h_i} \sim \exp(1)$ and $\rho_{l_j} \sim \exp(1)$. Hence, $P(\gamma_{h_i} \geq \theta_h | d_{h_i})$ in Eq. (18) is further deduced as

$$\begin{aligned} P(\gamma_{h_i} \geq \theta_h | d_{h_i}) &= P\left(\rho_{h_i} \geq \frac{\theta_h d_{h_i}^\delta (N_0 + P_s S_{\mathcal{H} \setminus \{h_i\}})}{P_s G_a}\right) \\ &= \exp\left(-\frac{\theta_h d_{h_i}^\delta (N_0 + P_s S_{\mathcal{H} \setminus \{h_i\}})}{P_s G_a}\right) \\ &= \exp\left(-\frac{\theta_h d_{h_i}^\delta N_0}{P_s G_a}\right) \mathbb{L}_{S_{\mathcal{H} \setminus \{h_i\}}}\left(\frac{\theta_h d_{h_i}^\delta}{G_a}\right). \end{aligned} \quad (21)$$

Let $\frac{\theta_h d_{h_i}^\delta}{G_a} = \Lambda_{h_i}$, and we have

$$\mathbb{L}_{S_{\mathcal{H} \setminus \{h_i\}}}\left(\frac{\theta_h d_{h_i}^\delta}{G_a}\right) = \mathbb{L}_{S_{\mathcal{H} \setminus \{h_i\}}}(\Lambda_{h_i}) = \mathbb{E}[e^{-\Lambda_{h_i} (S_{\mathcal{H} \setminus \{h_i\}})}], \quad (22)$$

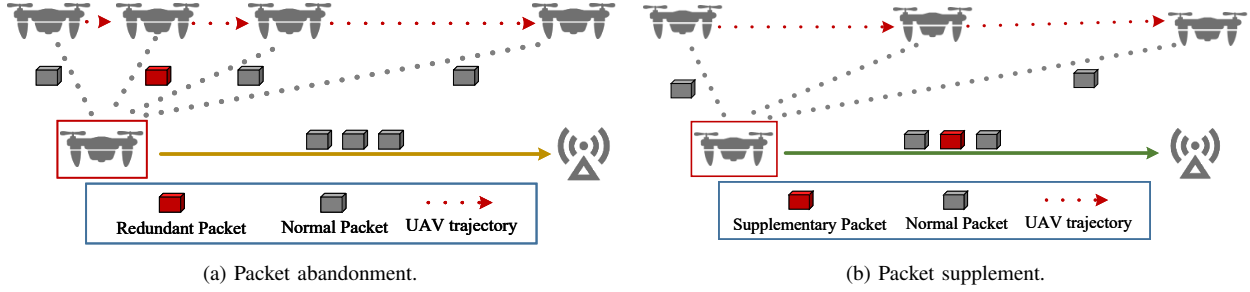


Fig. 5. On-board processing.

which is the Laplace transform of $S_{\mathcal{H}\setminus\{h_i\}}$. By substituting Eq. (12) into Eq. (22), we further derive

$$\begin{aligned}
 \mathbb{L}_{S_{\mathcal{H}\setminus\{h_i\}}}(\Lambda_{h_i}) &= \mathbb{E} \left[\exp \left(-\Lambda_{h_i} \sum_{h \in \mathcal{H}\setminus\{h_i\}} G_a \rho_h d_h^{-\delta} \right) \right] \\
 &\stackrel{\text{(a)}}{=} \mathbb{E} \left[\prod_{h \in \mathcal{H}\setminus\{h_i\}} \frac{1}{1 + \Lambda_{h_i} G_a d_h^{-\delta}} \right] \\
 &\stackrel{\text{(b)}}{=} \exp \left[-\lambda_h \int_{V_h} \left(1 - \frac{1}{1 + \Lambda_{h_i} G_a d_h^{-\delta}} \right) d(d_h) \right] \\
 &\stackrel{\text{(c)}}{=} \exp \left[-\lambda_h \int_{-L_x}^{L_x} \int_{-L_y}^{L_y} \int_0^{L_z} 1 - \frac{1}{1 + \Lambda_{h_i} G_a d_h^{-\delta}} dx dy dz \right] \\
 &\stackrel{\text{(d)}}{=} \exp(-\lambda_h \Theta_{h_i}). \tag{23}
 \end{aligned}$$

Wherein, **(a)** is obtained by the moment generating function, based on THEOREM 4.9 in [37]. **(b)** follows the probability generating function, based on eq. (90) in [38], which serves as a mathematical tool that converts the expectation of a continuous multiplication of functions into an integral over the PPP domain. Besides, d_h in **(b)** can be further expressed as $\sqrt{(x_h - x_{h_0})^2 + (y_h - y_{h_0})^2 + (z_h - z_{h_0})^2}$, demonstrated as **(c)**. Finally, Θ_{h_i} in **(d)** represents the triple integral in **(c)**, aiming to simplify the formula.

By substituting Eq. (21), (22) and (23) into (19), P_{cov}^i is calculated as

$$\begin{aligned}
 P_{cov}^i &= \int_0^\infty 4\pi\lambda_h d_h^2 \exp \left(\frac{-\theta_h d_h^\delta N_0}{P_s G_a} \right. \\
 &\quad \left. - \lambda_h \Theta_{h_i} - \frac{4}{3}\pi\lambda_h d_h^3 \right) d(d_h). \tag{24}
 \end{aligned}$$

The derivation processes of formulas aforementioned are also applicable to the calculations of coverage probability for sub-UAVs in low-altitude airspace V_l . Hence, the coverage probability of the j -th sub-UAV in \mathcal{L} is presented as

$$\begin{aligned}
 P_{cov}^j &= \int_0^\infty 4\pi\lambda_l d_l^2 \exp \left(\frac{-\theta_l d_l^\delta N_0}{P_s G_a} \right. \\
 &\quad \left. - \lambda_l \Theta_{l_j} - \frac{4}{3}\pi\lambda_l d_l^3 \right) d(d_l). \tag{25}
 \end{aligned}$$

V. ON-BOARD PROCESSING BASED ON MEC

During the real transmission of flight information, there are two abnormal conditions:

- Redundant flight packet: Packet of redundant information increases the calculation burden and causes trajectory overlap in the surveillance, further impairing the observability.
- Discontinuous flight packet: Packet loss due to error or collision leads to the discontinuity of trajectory, further impairing the observability.

If the trajectory optimization is solely entrusted to GS for completion, there exists a high probability that the packet loss will be aggravated owing to the long transmission distance, which further impairs the optimization performance. Consequently, we deploy MEC on the central UAV and propose an on-board processing mechanism. As such, we address the aforementioned two issues and achieve the timely optimization.

In short, the optimization objective is to improve the observability of trajectory monitoring, in order to help air traffic controllers visualize the flight path intuitively.

A. Packet Abandonment

Compared with the civil aircraft, UAV flies at a lower speed. Thus, UAV trajectories change slowly, so GS does not need to continuously receive position packets in short intervals. Meanwhile, abandoning redundant packets reduces the channel occupation of a single UAV, and improves the monitoring capacity of GS. As depicted in Fig. 5(a), after receiving two consecutive packets from the sub-UAV, the central UAV processes them. If the information of two packets is similar, the second packet is regarded as a redundant packet. Based on the on-board processing mechanism, the central UAV refuses to relay the redundant packet, which effectively prevents the overlap of trajectory on the surveillance and reduces the computing burden.

B. Packet Supplement

Due to the effect of path loss and channel shadowing, the packet loss occurs during the transmission [39]. Besides, on account of the limited processing capacity, the packet collision happens when multiple packets arrive at the central UAV simultaneously [6]. Generally, packet loss and collision cause the central UAV to miss packets. As illustrated in Fig. 5(b), after receiving two consecutive packets from the sub-UAV, the central UAV processes them. If the information of two packets is disparate, the second packet is regarded as a discontinuous

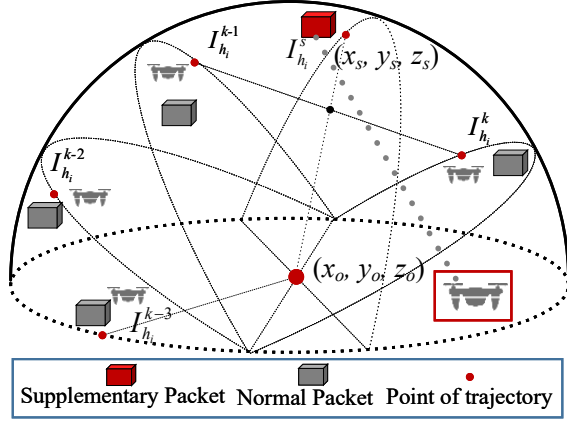


Fig. 6. Mechanism of supplement.

packet. Based on the on-board processing mechanism, the central UAV replenishes a supplementary packet, which ensures the continuous trajecorty of UAVs for the surveillance.

C. On-board Processing Mechanism

After receiving several position packets, GS generates the trajectory of the targeted UAV. When packets are continuously lost, GS clears the flight path of the UAV, and the UAV is deemed to leave the controlled airspace. For the flight surveillance, the position information is significant. We respectively leverage *Lon*, *Lat* and *Alt* to symbolize the longitude, latitude and altitude in a position packet. Hence, the position vector of the i -th high-altitude UAVs in the k -th packets can be classified as

$$I_{h_i}^k = [Lon_{h_i}^k, Lat_{h_i}^k, Alt_{h_i}^k]. \quad (26)$$

Similarly, the position vector of the j -th low-altitude UAVs in the g -th packets can be classified as

$$I_{l_j}^g = [Lon_{l_j}^g, Lat_{l_j}^g, Alt_{l_j}^g]. \quad (27)$$

The following mechanisms can be applied to $I_{h_i}^k$ of UAV h_i as well as $I_{l_j}^g$ of UAV l_j .

1) *Mechanism of Abandonment*: The central UAV records the first N position packets of the i -th sub-UAV and compute the Minkowski distances of adjacent position vectors in turns [40]. The Minkowski vector \mathcal{M}_{h_i} is defined as

$$\mathcal{M}_{h_i} = \{m_{h_i}^1, m_{h_i}^2, \dots, m_{h_i}^n, \dots, m_{h_i}^N\}. \quad (28)$$

The n -th Minkowski distance $m_{h_i}^n$ in \mathcal{M}_{h_i} is obtained as

$$m_{h_i}^n = (|Lon_{h_i}^{n+1} - Lon_{h_i}^n|^p + |Lat_{h_i}^{n+1} - Lat_{h_i}^n|^p + |Alt_{h_i}^{n+1} - Alt_{h_i}^n|^p)^{1/p}, \quad (29)$$

where p is the order of the Minkowski distances.

After receiving the k -th packet from h_i , the central UAV calculates the Minkowski distance $m_{h_i}^{k-1}$ between $I_{h_i}^k$ and $I_{h_i}^{k-1}$. If

$$m_{h_i}^{k-1} < \min\{m_{h_i}^1, m_{h_i}^2, \dots, m_{h_i}^n, \dots, m_{h_i}^N\}, \quad (30)$$

the central UAV records $m_{h_i}^{k-1}$ in \mathcal{M}_{h_i} , replaces the $\max\{m_{h_i}^1, m_{h_i}^2, \dots, m_{h_i}^n, \dots, m_{h_i}^N\}$, and abandons the k -th packet.

Algorithm 1 On-board processing algorithm

Input: N initial position vectors $I_{h_i}, I_{h_i}^k, I_{h_i}^{k-1}, I_{h_i}^{k-2}, I_{h_i}^{k-3}$.

Output: x_s, y_s , and z_s .

- 1: $\mathcal{M}_{h_i} \leftarrow \{0\}$.
- 2: $n \leftarrow 1$.
- 3: **while** $n \leq N$ **do**
- 4: Update $m_{h_i}^n$ based on Eq. (26) and (29).
- 5: Update \mathcal{M}_{h_i} based on Eq. (28).
- 6: $n \leftarrow n + 1$.
- 7: **end while**
- 8: Calculate $m_{h_i}^{k-1}$ by putting $I_{h_i}^k$ and $I_{h_i}^{k-1}$ into Eq. (26) and (29).
- 9: **if** $m_{h_i}^{k-1} < \min\{m_{h_i}^1, m_{h_i}^2, \dots, m_{h_i}^n, \dots, m_{h_i}^N\}$ **then**
- 10: Abandon $I_{h_i}^k$.
- 11: $\max\{m_{h_i}^1, m_{h_i}^2, \dots, m_{h_i}^n, \dots, m_{h_i}^N\} \leftarrow m_{h_i}^{k-1}$.
- 12: **end if**
- 13: **if** $m_{h_i}^{k-1} \geq \max\{m_{h_i}^1, m_{h_i}^2, \dots, m_{h_i}^n, \dots, m_{h_i}^N\}$ **then**
- 14: Calculate D by Eq. (32).
- 15: Calculate L by Eq. (33).
- 16: Calculate x_s, y_s and z_s by Eq. (35), (36), (37), (38).
- 17: Replenish $I_{h_i}^s$.
- 18: $\min\{m_{h_i}^1, m_{h_i}^2, \dots, m_{h_i}^n, \dots, m_{h_i}^N\} \leftarrow m_{h_i}^{k-1}$.
- 19: **end if**

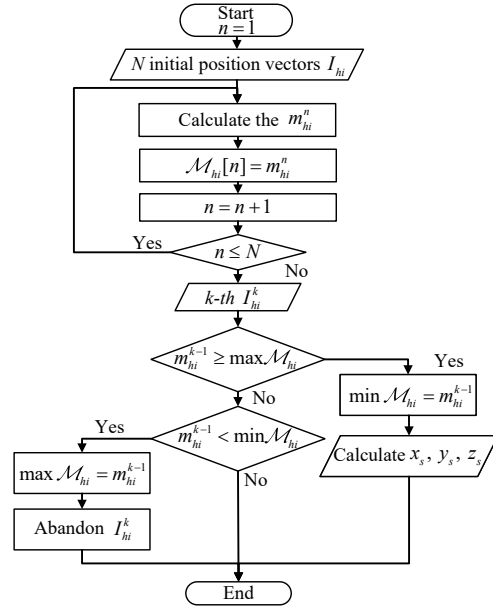


Fig. 7. On-board processing mechanism.

2) *Mechanism of Supplement*: If

$$m_{h_i}^{k-1} \geq \max\{m_{h_i}^1, m_{h_i}^2, \dots, m_{h_i}^n, \dots, m_{h_i}^N\}, \quad (31)$$

the central UAV records $m_{h_i}^{k-1}$ in \mathcal{M}_{h_i} , substitutes the $\min\{m_{h_i}^1, m_{h_i}^2, \dots, m_{h_i}^n, \dots, m_{h_i}^N\}$, and generates the packet supplement.

As shown in Fig. 6, we utilize $I_{h_i}^k, I_{h_i}^{k-1}, I_{h_i}^{k-2}$ and $I_{h_i}^{k-3}$ to find the circumscribed sphere. The supplementary position information is at the intersection of the sphere and the straight line which passes the center and midpoint between $I_{h_i}^k$ and

$I_{h_i}^{k-1}$, shown as the red cube in Fig. 6. Besides, the center is (x_o, y_o, z_o) . According to Cramer's Rule [41], the coefficient determinant $X = |\chi_1 \chi_2 \chi_3|$ is calculated as

$$\begin{vmatrix} Lon_{h_i}^k - Lon_{h_i}^{k-1} & Lat_{h_i}^k - Lat_{h_i}^{k-1} & Alt_{h_i}^k - Alt_{h_i}^{k-1} \\ Lon_{h_i}^{k-2} - Lon_{h_i}^{k-3} & Lat_{h_i}^{k-2} - Lat_{h_i}^{k-3} & Alt_{h_i}^{k-2} - Alt_{h_i}^{k-3} \\ Lon_{h_i}^{k-1} - Lon_{h_i}^{k-2} & Lat_{h_i}^{k-1} - Lat_{h_i}^{k-2} & Alt_{h_i}^{k-1} - Alt_{h_i}^{k-2} \end{vmatrix}. \quad (32)$$

The constant determinant $|B|$ is calculated as

$$|B| = \begin{vmatrix} \beta_1 \\ \beta_2 \\ \beta_3 \end{vmatrix}, \quad (33)$$

which is further deduced as

$$\begin{cases} \beta_1 = \{[(Lon_{h_i}^k)^2 - (Lon_{h_i}^{k-1})^2 + (Lat_{h_i}^k)^2 - (Lat_{h_i}^{k-1})^2 + (Alt_{h_i}^k)^2 - (Alt_{h_i}^{k-1})^2]\}/2, \\ \beta_2 = \{[(Lon_{h_i}^{k-2})^2 - (Lon_{h_i}^{k-3})^2 + (Lat_{h_i}^{k-2})^2 - (Lat_{h_i}^{k-3})^2 + (Alt_{h_i}^{k-2})^2 - (Alt_{h_i}^{k-3})^2]\}/2, \\ \beta_3 = \{[(Lon_{h_i}^{k-1})^2 - (Lon_{h_i}^{k-2})^2 + (Lat_{h_i}^{k-1})^2 - (Lat_{h_i}^{k-2})^2 + (Alt_{h_i}^{k-1})^2 - (Alt_{h_i}^{k-2})^2]\}/2. \end{cases} \quad (34)$$

Moreover, the coordinate of center is deduced as

$$x_o = \frac{|B \chi_2 \chi_3|}{X}, \quad y_o = \frac{|\chi_1 B \chi_3|}{X}, \quad z_o = \frac{|\chi_1 \chi_2 B|}{X}, \quad (35)$$

and the radius r is

$$r = \sqrt{(x_o - Lon_{h_i}^k)^2 + (y_o - Lat_{h_i}^k)^2 + (z_o - Alt_{h_i}^k)^2}. \quad (36)$$

The position information in the supplementary packet between $I_{h_i}^k$ and $I_{h_i}^{k-1}$ is obtained by combining the following two equations:

$$(x_s - x_o)^2 + (y_s - y_o)^2 + (z_s - z_o)^2 = r^2, \quad (37)$$

and

$$\begin{aligned} & \frac{x_s - x_o}{(Lon_{h_i}^k + Lon_{h_i}^{k-1})/2 - x_o} \\ &= \frac{y_s - y_o}{(Lat_{h_i}^k + Lat_{h_i}^{k-1})/2 - y_o} \\ &= \frac{z_s - z_o}{(Alt_{h_i}^k + Alt_{h_i}^{k-1})/2 - z_o}. \end{aligned} \quad (38)$$

In detail, the on-board processing mechanisms are further described in Algorithm 1, and the corresponding flowchart is shown as Fig.7.

VI. SIMULATION RESULTS AND ANALYSIS

To evaluate the detailed performance, MATLAB is employed to simulate the 3D PPP distribution scenario of the sub-UAVs and central UAVs, as shown in Fig. 8. The green icons representing UAVs in high-altitude airspace and yellow icons denoting UAVs in low-altitude airspace, are separated by the blue isolation layer, whose thickness H_0 is 1km. The circle, diamond, and triangle symbolize the sub-UAV, central UAV, and GS, respectively. The thickness of both airspace ΔH is fixed as 4.5km. Besides, the height of GS is set as 50m. The working frequency of the 5G system and ADS-B system is set

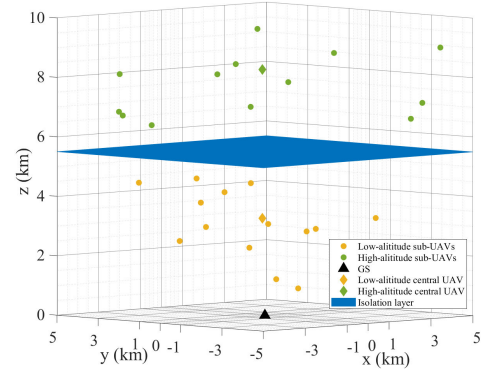


Fig. 8. Simulation scenario.

TABLE II
KEY PARAMETERS IN THE SIMULATIONS

Parameter	Value	Parameter	Value
f_{5G}	3.5GHz	f_{ADS-B}	1090MHz
λ_{5G}	0.0857m	λ_{ADS-B}	0.2752m
B_{5G}	100MHz	B_{ADS-B}	1MHz
n_0	-174dBm/Hz	δ	2~4.9
P_s	1W~20W	σ	5×10^3
P_{ch}	20W	P_{cl}	20W
G_g	20dBi	G_a	23dBi
θ_h	-14dB~-7dB	θ_l	-14dB~-7dB
λ_l	1~60	λ_h	1~60
ΔH	4.5km	H_0	1km
H_G	50m	ε_r	15

as 3.5GHz and 1090MHz, respectively [42]. The wavelength λ_{5G} is 0.0857m and λ_{ADS-B} is 0.2752m, according to $\lambda=c/f$. Moreover, the bandwidth B_{5G} and B_{ADS-B} are set as 100MHz and 1MHz, respectively [6]. The transmitting power of the central UAVs are fixed as 20W while the transmitting power of the sub-UAVs varies in [1W, 20W]. In the wireless communication system, the value of Rice factor is usually determined according to the actual situation. Supposing fixing SNR, a larger Rice factor contributes to a smaller bit error rate, and a better system performance [43]. Therefore, we take the Rice factor as 3 in the A2G channel, which comprehensively simulates the influence of reflected signals. Other parameters in simulations are listed in TABLE II.

A. Performance Analysis of A2G channel

We verify the network performance of the A2G channel by Eq. (9) and (10), which pertinently describe the process of signal transmission [44]. The related indexes can be further subdivided into $PL_l = -10\log(P_G/P_{cl})$, $PL_h = -10\log(P_G/P_{ch})$, ϖ_l and ϖ_h .

Fig. 9 and Fig. 10 depict the A2G channel performance for the low-altitude central UAV l_0 . In Fig. 9, the black solid line indicates the path loss without Rice fading while the red dotted line demonstrates the path loss with Rice fading. The thick lines are corresponding nonlinear fitting curves. From Fig. 9, the A2G models are oscillation models, following the law of free space path loss. With the height H_l of the central UAV l_0 increasing, the path loss PL_l also increases. After the introduction of Rice fading, PL_l is growing, but the increment

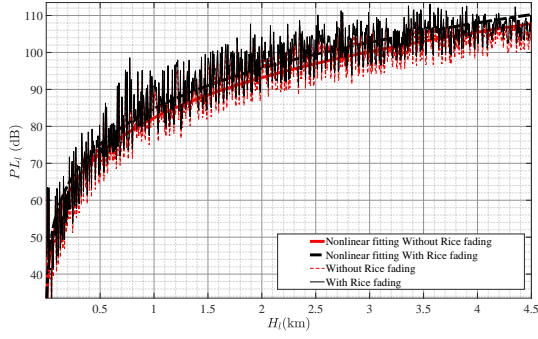


Fig. 9. Relationship between the H_l and PL_l .

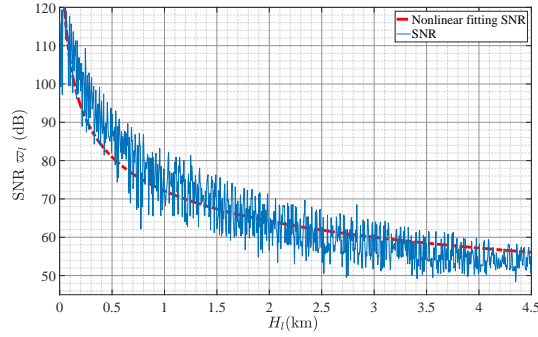


Fig. 10. Relationship between the H_l and ϖ_l .

is not obvious in the low-altitude airspace. When H_l is greater than 4km, the PL_l curve tends to be smooth. In Fig. 10, the blue solid line indicates the SNR of signal from l_0 to GS and the red dotted line is the corresponding nonlinear fitting. With the height H_l of the central UAV l_0 increasing, the SNR ϖ_l decreases. However, the decay speed of ϖ_l gradually lowers with the addition of H_l . The curve tends to be flat when H_l is higher than 4km in the 5G scenario. When H_l approaches 0, the value of PL_l changes abruptly. This is accounted that when H_l is much less than the horizontal distance between l_0 and GS, the multi-rays transmitting model degenerates into a single-ray transmitting model. The height of the central UAV l_0 is recommended to be limited in respect to the practical receiving threshold of GS.

Fig. 11 and Fig. 12 illustrate the A2G channel performance for the high-altitude central UAV h_0 . In Fig. 11, the black solid line represents the path loss without Rice fading while the red dotted line symbolizes the path loss with Rice fading. The thick lines are corresponding nonlinear fitting curves. It is observed from Fig. 11 that PL_h magnifies as H_l enlarges, but the increment is not obvious in the high-altitude airspace in respect to the ADS-B central UAV h_0 . Further, the difference between with and without Rice fading is obvious in the high-altitude airspace. Since we limit the height of the central UAV h_0 within (5.5km, 10km), the growth of PL_h does not exhibit a smooth trend. In Fig. 12, the blue solid line expresses the SNR of signal from h_0 to GS and the red dotted line is the corresponding nonlinear fitting. With the height H_h of the central UAV h_0 rising, the SNR ϖ_h reduces. Similarly, the decrement is small in the ADS-B scenario. The height of the

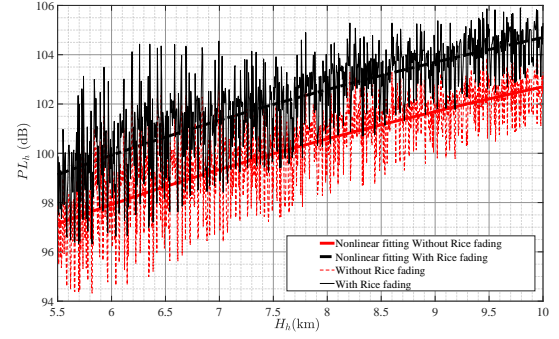


Fig. 11. Relationship between the H_h and PL_h .

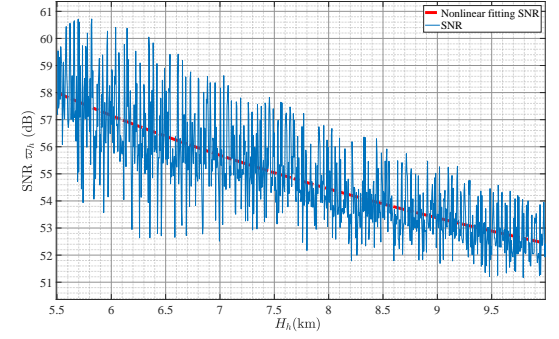


Fig. 12. Relationship between the H_h and ϖ_h .

central UAV h_0 should be determined according to the actual requirement of GS.

B. Performance Analysis of A2A Channel

Fig. 13a shows the relationship between the density of sub-UAVs and averaged SINR of the signal received by the central UAV. Both airspaces have the same size, and all sub-UAVs send packets to the central UAVs, so the performance analysis of the A2A does not distinguish between the high-altitude and the low-altitude. As the density of sub-UAVs increases, the averaged SINR decreases. Besides, the simulation results coincide with the theoretical results, which validates the accuracy of theoretical analysis. The increment of sub-UAVs leads to abundant signals propagating in the airspace. Thus, there exist more interference signals when the central UAV receives a specific signal. When the density of sub-UAVs exceeds 40, the averaged SINR of the signals degenerates to around -20, which is harmful to signal processing. Therefore, the density of sub-UAVs should adapt to practical received threshold.

Fig. 13b describes the relationship between the coverage probability and transmitting power of sub-UAVs under different received thresholds. Besides, the simulation results coincide with the theoretical results, which validates the accuracy of theoretical analysis. Moreover, the received threshold increases with the direction of the arrow. The path loss index and density are set as 2 and 20, respectively. With the power rising, the signal coverage probability grows. Besides, when the power is greater than 17W, it shows a smooth trend in the increment of the coverage probability regardless of thresholds. However, the enlargement of the threshold leads

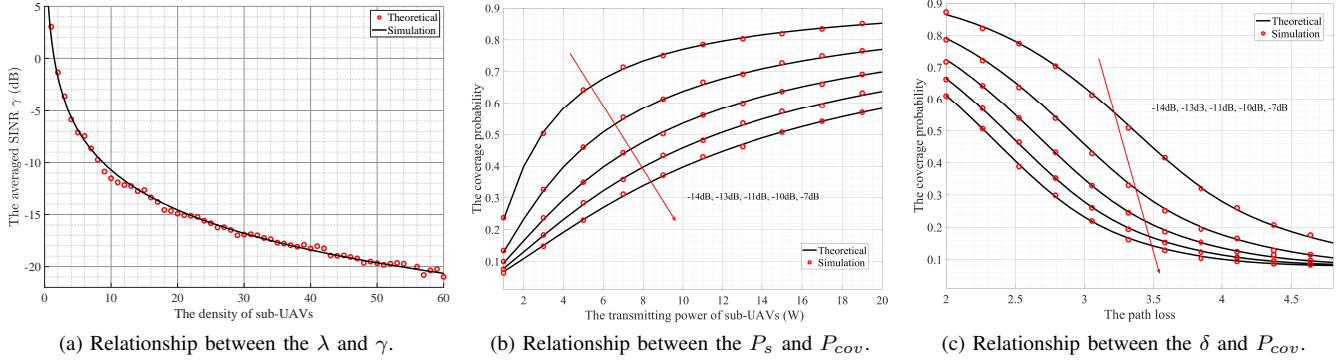


Fig. 13. Performance analyze of A2A.

to the coverage probability falling. Supposing the threshold is -14dB , fixing the transmitting power as 7W makes the highest efficiency of energy investment, since the gain of the coverage probability from the increment of a unit transmitting power is continuously decreasing.

Fig. 13c presents the relationship between the coverage probability and path loss index under different received thresholds. The transmitting power and density are fixed as 20W and 20 , respectively. Besides, the simulation results coincide with the theoretical results, which validates the accuracy of theoretical analysis. Moreover, the received threshold increases with the direction of the arrow. When the path loss index is less than 2.5 , its effect on the decrement of the coverage probability is relatively small. However, when the path loss is greater than 2.5 , the performance of the communication system deteriorates dramatically. When the path loss is greater than 4 , only in the scenario of -14dB threshold, the coverage probability is still relatively considerable. However, in the other four cases, the coverage probability approaches 0.1 . In the above four cases, the system performance can only be improved by lowering the threshold, intensifying the transmitting power or reducing the density of sub-UAVs.

C. Experiments of On-board Processing Algorithm

As shown in Fig. 14, we collect the actual flight data of the UAV for algorithm verification. **A** is the UAV equipped with 5G module (SIM8262E-M2), while **B** is the UAV equipped with ADS-B out device (PT050X). Additionally, **C** is the Raspberry PI (4-Model-B), playing the role of GS and processing the position packets. **D** is the Realtek software defined radio as the antenna to receive the position packets. Besides, **E** is the display and **F** is the UAV controller. The constructions of the sending and receiving terminals are built in our lab. Further, in the experiment, we consider A and B as sub-UAVs and C as the central UAV.

Fig. 15 demonstrates the on-board data processing of position packets. Based on the mechanism, the central UAV processes the position packets of the sub-UAVs accordingly after receiving, and then transmits the packets to GS. On the one hand, there exist random perturbations or similar information during positioning and transmission. Relaying these redundant information to GS aggravates the burden of data

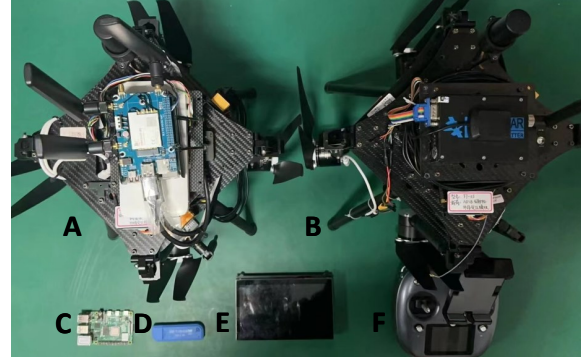


Fig. 14. Experimental equipments.

processing, which is time-consuming and energy-consuming. Therefore, we utilize the packet abandonment mechanism to reduce the redundant information. On the other hand, the packets transmission is affected by many random factors, leading to packet error or loss in serious cases. Further, the above situations trigger discontinuous trajectory, thus decreasing the observability. Therefore, we use the packet supplement mechanism to replenish a supplementary packet, achieving a smooth display of the UAV trajectory. Data ① is actual flight packets, but this scenario is not universal, since the altitude of the UAV does not change continuously. Therefore, we collect simulation data of ② and ③ for additional verifications.

Fig. 15(a) and Fig. 15(b) show the original data and optimized data of trajectory ①. The dots represent the received position packets, and the triangles represent the supplementary packets. In this scenario, the redundant data is effectively reduced by 52.55% , and 20 packets are added, accounting for 14.39% of the optimized data. However, trajectory ① is a special case, since the altitude stays invariable for most of trajectories. Therefore, the spherical supplement mechanism is ineffective in this scenario. Instead, the weighted average is used for the supplement, which means we utilize adjacent points to perform the linear supplement.

Fig. 15(c) and Fig. 15(d) display the original data and optimized data of trajectory ②. In this scenario, the longitude, latitude and altitude of the UAV change over time, which is a more universal scene. Therefore, the spherical supplement mechanism is adopted. In trajectory ②, the redundant data

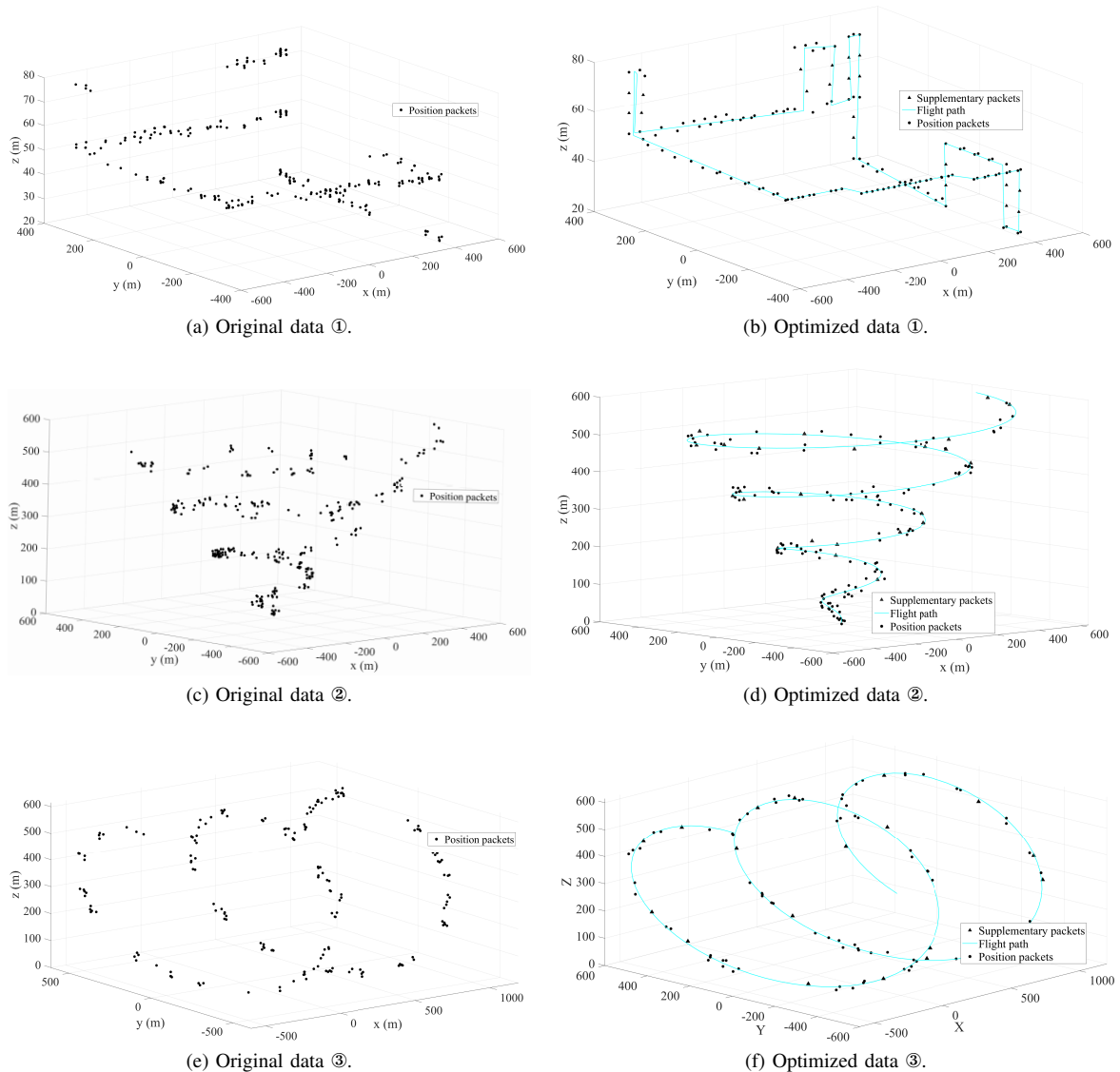


Fig. 15. On-board data processing of position packets.

is effectively reduced by 52.41%, and 26 packets are added, accounting for 16.05% of the optimized data.

Fig. 15(e) and Fig. 15(f) illustrate the original data and optimized data of trajectory ③. In this scenario, the longitude, latitude and altitude of the UAV also change over time. Therefore, the spherical supplement mechanism is adopted. In trajectory ③, the redundant data is effectively reduced by 55.49%, and 19 packets are added, accounting for 18.81% of the optimized data.

However, the algorithm sacrifices accuracies to some extent in two unusual cases. In particular, the first case is that the altitude of UAV remains unchanged for an extended period. Besides, the second case is that the velocity of UAV undergoes a transient change.

VII. CONCLUSIONS

In this paper, we design the cooperating framework of ADS-B in B5G for hierarchical UAV networks. Moreover, since the redundancy or trajectory information loss during

transmission aggravates the performance and decreases the observability, the MEC based on-board processing algorithm is proposed. In detail, we build the system of the A2G and A2A channels based on the deterministic modeling and stochastic modeling, respectively. Besides, we derive the related analytic formulas, analyze the performance of the A2G and A2A systems, and provide the corresponding suggestions about the height, density and transmitting power of UAVs. Further, the algorithm is verified by simulations as well as experiments. The results indicate that the proposed mechanism effectively filters out redundant data with similar information and makes supplies for the discontinuities.

In future works, we will conduct more real-world experiments. Moreover, we will build a multi-mode hybrid network for UAVs based on more access methods. Furthermore, considering the hybrid network, we will explore how to enable GS to dynamically combine the multi-source heterogeneous data, thus offering more solid assurance and robust support

for low-altitude development.

REFERENCES

- [1] J. Kang, J. Chen, M. Xu, Z. Xiong, Y. Jiao, L. Han, D. Niyato, Y. Tong and S. Xie, "UAV-Assisted Dynamic Avatar Task Migration for Vehicular Metaverse Services: A Multi-Agent Deep Reinforcement Learning Approach," *IEEE/CAA J. Autom. Sinica*, vol. 11, no. 2, pp. 430-445, Feb. 2024.
- [2] Z. Jia, J. You, C. Dong, Q. Wu, F. Zhou, D. Niyato and Z. Han, "Co-operative Cognitive Dynamic System in UAV Swarms: Reconfigurable Mechanism and Framework," *IEEE Veh. Technol. Mag.*, vol. 19, no. 3, pp. 90-101, Sep. 2024.
- [3] Y. Zhu, Z. Jia, Q. Wu, C. Dong, Z. Zhuang, H. Hu and Q. Cai, "UAV Trajectory Tracking via RNN-enhanced IMM-KF with ADS-B Data," in *IEEE Wireless Commun. Networking Conf.*, Dubai, United Arab Emirates, Apr. 2024.
- [4] C. Dong, Y. Zhang, Z. Jia, Y. Liao, L. Zhang and Q. Wu, "Three-dimension collision-free trajectory planning of UAVs based on ADS-B information in low-altitude urban airspace," *Chinese J. Aeronaut.*, 2024.
- [5] Y. Liao, L. Zhang, Z. Jia, C. Dong, Y. Zhang, Q. Wu, H. Hu and B. Wang, "Impact of UAVs Equipped with ADS-B on the Civil Aviation Monitoring System," in *IEEE Int. Conf. Commun. China*, Dalian, China, Aug. 2023.
- [6] D. Zhou, M. Sheng, J. Li and Z. Han, "Aerospace Integrated Networks Innovation for Empowering 6G: A Survey and Future Challenges," *IEEE Commun. Surveys Tuts.*, vol. 25, no. 2, pp. 975-1019, second quarter, 2023.
- [7] K. Yan, L. Ma and Y. Zhang, "Research on the Application of 5G Technology in UAV Data Link," in *Int. Inf. Technol. Artif. Intell. Conf.*, Chongqing, China, Dec. 2020.
- [8] J. Wang, Y. Liu, S. Niu and H. Song, "Extensive Throughput Enhancement For 5G-Enabled UAV Swarm Networking," *IEEE J-MASS*, vol. 2, no. 4, pp. 199-208, Dec. 2021.
- [9] R. Lai, B. Zhang, G. Gong, H. Yuan, J. Yang, J. Zhang, and M. Zhou, "Energy-Efficient Scheduling in UAV-Assisted Hierarchical Wireless Sensor Networks," *IEEE Internet Things J.*, vol. 11, no. 11, pp. 20194-20206, Jun. 2024.
- [10] Y. Su, J. Zhou and Z. Guo, "A Trust-Based Security Scheme for 5G UAV Communication Systems," in *Int. Conf. Dependable, Auton. Secur. Comput.*, Calgary, AB, Canada, Aug. 2020.
- [11] Z. Jia, Q. Wu, C. Dong, C. Yuen, and Z. Han, "Hierarchical aerial computing for Internet of things via cooperation of HAPs and UAVs," *IEEE Internet Things J.*, vol. 10, no. 7, pp. 5676-5688, Apr. 2023.
- [12] H. Yuan, M. Wang, J. Bi, S. Shi, J. Yang, J. Zhang, M. Zhou, and R. Buyya, "Cost-Efficient Task Offloading in Mobile Edge Computing With Layered Unmanned Aerial Vehicles," *IEEE Internet Things J.*, vol. 11, no. 19, pp. 30496-30509, Oct. 2024.
- [13] Q. Zhang, J. Chen, L. Ji, Z. Feng, and Z. Chen, "Response delay optimization in mobile edge computing enabled UAV swarm," *IEEE Trans. Veh. Technol.*, vol. 69, no. 99, pp. 3280-3295, Mar. 2020.
- [14] Y. K. Tun, Y. M. Park, N. H. Tran, W. Saad, S. R. Pandey and C. S. Hong, "Energy-Efficient Resource Management in UAV-Assisted Mobile Edge Computing," *IEEE Commun. Lett.*, vol. 25, no. 1, pp. 249-253, Jan. 2021.
- [15] Y. Qu, H. Sun, C. Dong, J. Kang, H. Dai, Q. Wu and S. Guo, "Elastic Collaborative Edge Intelligence for UAV Swarm: Architecture, Challenges, and Opportunities," *IEEE Commun. Mag.*, vol. 62, no. 1, pp. 62-68, Jan. 2024.
- [16] W. Khawaja, I. Guvenc, D. W. Matolak, U. Fiebig and N. Schneckenburger, "A Survey of Air-to-Ground Propagation Channel Modeling for Unmanned Aerial Vehicles," *IEEE Commun. Surveys Tuts.*, vol. 21, no. 3, pp. 2361-2391, third quarter, 2019.
- [17] Z. Shao, M. Chen, A. S. Avestimehr and S. R. Li, "Cross-Layer Optimization for Wireless Networks With Deterministic Channel Models," *IEEE Trans. Inform. Theory*, vol. 57, no. 9, pp. 5840-5862, Sep. 2011.
- [18] Y. Guo, Y. Zhang, L. Pang, X. Huang, P. Ren and Y. Chen, "Antenna Topology Optimization for Massive MIMO Near-Field Wireless Communications with Line-of-Sight Deterministic Channels," in *Int. Symp. Person Indoor Mobile Radio Commun.*, Toronto, ON, Canada, Sep. 2023.
- [19] J. G. Andrews, F. Baccelli and R. K. Ganti, "A Tractable Approach to Coverage and Rate in Cellular Networks," *IEEE Trans. Commun.*, vol. 59, no. 11, pp. 3122-3134, Nov. 2011.
- [20] Y. Liao, Z. Jia, C. Dong, L. Zhang, Q. Wu, H. Hu and Z. Han, "Interference Analysis for Coexistence of UAVs and Civil Aircrafts Based on Automatic Dependent Surveillance-Broadcast," *IEEE Trans. Veh. Technol.*, vol. 73, no. 10, pp. 15911-15915, Oct. 2024.
- [21] Y. Zhu, J. He, Z. Jia, Q. Wu, C. Dong and L. Zhang, "ADS-B and Remote ID Based Performance Analysis for UAV Surveillance in Low-Altitude Intelligent Networks," *Journal of Data Acquisition & Processing*, Oct. 2024.
- [22] R. Raheb, S. James, A. Hudak and A. Lacher, "Impact of Communications Quality of Service (QoS) on Remote ID as an Unmanned Aircraft (UA) Coordination Mechanism," in *IEEE AIAA Dig. Avionics Syst. Conf.*, San Antonio, TX, USA, 2021.
- [23] Y. He, D. Zhai, Y. Jiang and R. Zhang, "Relay Selection for UAV-Assisted Urban Vehicular Ad Hoc Networks," *IEEE Wirel. Commun. Lett.*, vol. 9, no. 9, pp. 1379-1383, Sep. 2020.
- [24] S. Gupta, J. K. Mohanta and A. Jaleel, "Design of Path Tracking Control and Flying Ad-hoc Network Rejoin Policy in Multi-UAV System," in *Int. Conf. Control. Commun. Comput.*, Thiruvananthapuram, India, 2023.
- [25] Z. Jia, M. Sheng, J. Li, D. Niyato, and Z. Han, "LEO-satellite-assisted UAV: Joint trajectory and data collection for Internet of remote things in 6G aerial access networks," *IEEE Internet Things J.*, vol. 8, no. 12, pp. 9814-9826, Sep. 2021.
- [26] V. Roberge, M. Tarbouchi and G. Labonte, "Comparison of Parallel Genetic Algorithm and Particle Swarm Optimization for Real-Time UAV Path Planning," *IEEE Trans. Ind. Inform.*, vol. 9, no. 1, pp. 132-141, Feb. 2013.
- [27] J. Yuan, H. Wang, Y. Chen, Z. Qin, L. Zhang, and W. Sun, "Relay Selection Based on Location Prediction in Collaborative Communication," in *Int. Conf. Commun. Technol. Proc.*, Nanning, China, Oct. 2020.
- [28] J. Zhang, Z. Shi, A. Zhang, Q. Yang, G. Shi and Y. Wu, "UAV Trajectory Prediction Based on Flight State Recognition," *IEEE Trans. Aero. Elec. Sys.*, vol. 60, no. 3, pp. 2629-2641, Jun. 2024.
- [29] Y. Duan, C. Zheng, H. Xi and J. Zhang, "Research on ADS-B Signal Noise Reduction Based on EEMD-PE," *Radio Engineering*, vol. 53, no. 7, pp. 1734-1740, Jul. 2023.
- [30] S. Sciancalepore and R. D. Pietro, "SOS: Standard-Compliant and Packet Loss Tolerant Security Framework for ADS-B Communications," *IEEE Trans. Depend. Secure*, vol. 18, no. 4, pp. 1681-1698, Jul. 2021.
- [31] SBS Base Station. [Online]. Available: //woodair.net/SBS/Article/Bare-bones42_Socket_Data.htm
- [32] D. W. Matolak and R. Sun, "Air-Ground Channel Characterization for Unmanned Aircraft Systems—Part I: Methods, Measurements, and Models for Over-Water Settings," *IEEE Trans. Veh. Technol.*, vol. 66, no. 1, pp. 26-44, Jan. 2017.
- [33] Cosine Rule. [Online]. Available: //www.geekforgeeks.org/cosine-rule/
- [34] Int. Telecommun. Union, "Propagation data and prediction methods required for the design of terrestrial line-of-sight systems," Geneva, Switzerland, Rec. ITU-R P. 530-14, Feb. 2012.
- [35] Y. Guo, X. Jia, S. Cao and Z. Hao, "Analysis of Downlink Coverage and Capacity for 3D Mobile UAV Networks," in *IEEE Int. Symp. Mechatronics Ind. Informatics*, Zhuhai, China, Jan. 2021.
- [36] X. Liu, "Closed-Form Coverage Probability in Cellular Networks with Poisson Point Process," *IEEE Trans. Veh. Technol.*, vol. 68, no. 8, pp. 8206-8209, Aug. 2019.
- [37] M. Haenggi, "Stochastic Geometry for Wireless Networks". New York, NY, USA: Cambridge Univ. Press, 2013.
- [38] H. E. Sawy, A. S. Salem, M. Alouini and M. Z. Win, "Modeling and Analysis of Cellular Networks Using Stochastic Geometry: A Tutorial," *IEEE Commun. Surveys Tuts.*, vol. 19, no. 1, pp. 167-203, first quarter, 2017.
- [39] T. Mahmood, W. Q. Mohamed and O. A. Imran, "Factors Influencing the Shadow Path Loss Model with Different Antenna Gains Over Large-Scale Fading Channel," in *Int. Conf. Artif. Intell. Mechatronics Syst.*, Bandung, Indonesia, 2021.
- [40] H. Xu, W. Zeng, X. Zeng and G. G. Yen, "An Evolutionary Algorithm Based on Minkowski Distance for Many-Objective Optimization," *IEEE Trans. Cybernetics*, vol. 49, no. 11, pp. 3968-3979, Nov. 2019.
- [41] R. E. Klein, "Teaching linear systems theory using Cramer's rule," *IEEE Trans. Educ.*, vol. 33, no. 3, pp. 258-267, Aug. 1990.
- [42] F. Ali, M. Salih and M. Ilyas, "MIMO Patch Antenna with Metamaterial 3.5GHz for 5G Applications," in *Int. Conf. Adv. Electr. Comput., Commun. Sustain. Technol.*, Bhilai, India, 2022.
- [43] T. Mahjoub, A. B. Mnaouer, H. Boujemaa and M. B. Said, "Performance Analysis of LoRa for Rice Fading Channels," in *Int. Symp. Networks, Comput. Commun.*, Doha, Qatar, Oct. 2023.
- [44] Z. Rezki and M. Alouini, "On the Capacity of Nakagami-m Fading Channels with Full Channel State Information at Low SNR," *IEEE Wire. Commun. Lett.*, vol. 1, no. 3, pp. 253-256, Jun. 2012.